

Surge impact behavior of granular flows: effects of water content

Abstract Understanding the fundamental dynamics of interaction between multi-phase geophysical flows and engineering structures is crucial for mitigating geophysical hazards. Specifically, liquid phase between particles induces matric suction which could play a significant part in regulating flow dynamics and warrants further consideration. In this study, flume model tests were conducted to investigate the effects of water content (0–30%) on the impact behavior of granular flows. The particle image velocimetry technique was adopted to visualize the impact kinematics and the impact force was measured through a model barrier system. Results revealed that, besides geometric effects (kinetic sieving), mechanical effects (shearing and collision) are also vital for the mechanism of reverse segregation. At higher water contents, 20 and 30% in this study, discrete-surge impact, rather than a progressive impact process, was observed. The discrete surges induce impulses on the barrier. The discrete surges result from self-organization of unsaturated granular flows to overcome the enhanced shear strength induced by matric suction. Finally, a dimensionless index, namely the suction number, is used to quantify the effect of suction on the dynamic behavior of granular flows. Even for large-scale geophysical flows, if the content of fine particles is high, effect of suction should not be neglected.

Keywords Granular flows · Impact behavior · Water content · Discrete surges · Matric suction

Introduction

Gravity-driven flows of an assembly of granular particles have attracted increasing interest, as they are useful for understanding a wide variety of geomorphological and industrial processes (Mills et al. 1999; Armanini et al. 2005). Granular (mass) flow (e.g., granular/rock/debris avalanches, debris flows, and pyroclastic flows) are geological phenomena of great concern because they often cause catastrophic disasters with significant economic impacts due to the long run-out distance and large destructive forces in mountainous regions. They occur when masses of poorly sorted sediment, agitated and mixed with water (saturated debris for most “debris flows” and partially saturated debris for “granular/rock/debris avalanches”), and surge down slopes in response to gravitational attraction (Iverson 1997; Hungr et al. 2014; Chen et al. 2013). Granular flows are different from sediment-laden water floods in that both solid and fluid forces influence the motion and govern their rheological properties (Iverson 1997). Granular materials can vary greatly depending on the geometry of the grains and the nature of their interactions. For simplicity, numerical and laboratory simulations are typically restricted to assemblies of spherical, slightly polydispersed cohesionless grains (particulate study) which usually do not have an interstitial fluid (e.g., Savage and Sayed 1984; Campbell 1990; Goldhirsch 2003; MiDi 2004; Da Cruz et al. 2005; Zhou and Ng 2010) or focusing on the extreme condition, i.e., cohesionless solid particles fully saturated by pure water (Bagnold 1954; Armanini et al. 2008). However, granular

flows in nature (geophysical flows) are finite and contiguous bodies of solid and fluid that move coherently (Iverson and Vallance 2001). They are often not cohesionless and may have apparent cohesion (matric suction for unsaturated conditions) from the liquid phase.

Cost-effective design of debris-resisting structures still remains challenging, owing to the complex properties of granular flows themselves. In order to simplify the flow type and reveal the mechanisms of debris-structure interaction, extensive experimental modeling has been carried out to investigate the dynamic impact process and the impact load evolution using dry granular flows (Choi et al. 2015; Koo et al. 2017). Due to the high grain contact shear strength, dry granular flows result in an attenuating pile-up mechanism (Choi et al. 2015) and interact with the barrier in a continuous manner. Typically, no impulse peak load can be observed from the impact time history. The formation of dead zone at the base of barrier indicates that the total force may be dominated by the static load. The debris-resisting barriers may only be required to intercept the dynamic flow front as the subsequent flow energy may mainly be dissipated through internal shearing (Ng et al. 2016). However, there still lacks an effective approach for probing the internal structure and velocity field along the flow depth. As a result, the current impact models are generally semi-empirical. Furthermore, particle size distribution can have a major influence on the local rheology and mobility of geophysical flows (Gray and Chugunov 2006; Johnson et al. 2012) through the effects of reverse segregation. To explain the “reverse” phenomena, numerous models have been proposed, e.g., the kinetic sieving model and squeeze expulsion mechanism (Savage and Lun 1988). So far, the mechanism of reverse segregation during the granular impact process on a barrier remains poorly understood.

The research on mobility and impact of dry (e.g., debris avalanche) and saturated granular flows (e.g., debris flows) has been intensively conducted (Law et al. 2015; Davies and McSaveney 1999; Bugnion et al. 2012; Kwan et al. 2014; Wendeler 2016). Current design approaches used to estimate impact load treat geophysical flows as equivalent fluids without considering solid-fluid interaction. Due the regulation of pore pressure on the overall flow behavior (Iverson 1997; Iverson and George 2014), the impact of saturated mixtures on a barrier is characterized with much higher impact height and impact force. What should be emphasized is that most “granular/rock/debris avalanches” in nature are partially saturated (multi-phases) and the liquid phase between particles is not continuous. Also, some natural overly-steep soil slopes are primarily maintained by the matric suction. Failure of such slopes would occur under certain rainfall or ground motion (earthquake) conditions, resulting in unsaturated granular flows. Even for the notional saturated debris flows, the frontal head can be generally considered to be unsaturated (Iverson et al. 2010), owing to the effects of longitudinal segregation along the flow path. The induced matric suction of the unsaturated mixtures would

undoubtedly enhance the internal shear strength and thus reduce the mobility (Zhou et al. 2016). One may postulate that the enhanced shear strength would further reduce the impact loads on protective structures. However, the effects of water content at the unsaturated range on the impact behavior are rarely investigated experimentally.

In this paper, granular flows of varying water contents (mainly the unsaturated range: 0–30%) were adopted to impact an instrumented barrier in an inclined flume. The dynamic response of barrier during impact and deposition processes was investigated. The relationship between water content and granular flow impact pattern was preliminarily elucidated.

Flume model test

Model setup

In order to study the impact behavior of granular materials with different water contents, an inclined flume with a barrier was adopted (Fig. 1a). The flume model has dimensions of 4.4 m in length, 0.4 m in width, and 0.6 m in height. The flume inclination was fixed at 35° for this study. The flume bed was coated by self-adhesive plastic sheets with interface friction angle of 22.5° (Ng

et al. 2015). The interface friction angle was measured in the laboratory using the method described by Savage and Hutter (1989). Granular materials were placed into a paper cylinder on the flume bed. The flume was inclined until the paper cylinder began sliding. The flume inclination at which the cylinder began to slide is the interface friction angle. Side wall of the flume comprised Perspex windows which enable high-speed cameras to capture the impact behavior (Fig. 1b). Illumination was provided using two LED lights. A pneumatic gate controls the release of debris materials and is connected to the data logger to trigger the initiation of the tests.

An aluminum plate (500 mm in height and 400 mm in width) was installed at the end of the transportation zone to act as the barrier (Fig. 1b). The plate was mounted using four screws encapsulated by high-stiffness springs. The barrier system was designed to use bearings to minimize the effects of tilting (eccentric loading).

Instrumentation

The impact kinematics was captured using a high-speed camera at a frame rate of 250 fps and resolution of 480×420 px. The influence of water content on velocity field and impact processes

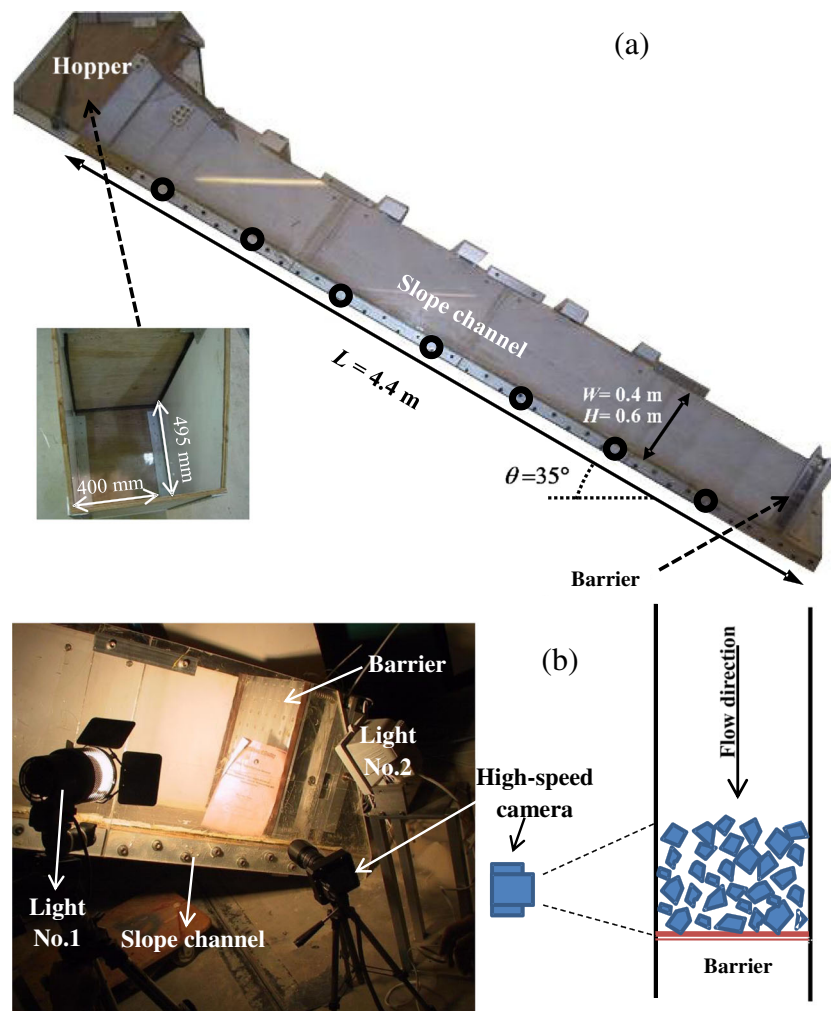


Fig. 1 Setup of physical model test. a Slope channel. b The high-speed camera installed at the sidewall for capturing particle trajectories and contact behavior

in front of the barrier can be analyzed using particle image velocimetry (PIV) analysis (White et al. 2003; Take 2015).

The non-uniformly distributed impact pressure along the barrier height induces eccentric loading on the measurement system. To overcome the disadvantage of eccentric loading, a combination of high-stiffness springs and laser sensors, instead of single load cell was adopted to deduce the impact force. However, the movable barrier in front of the springs unavoidably results in inertial effect on the measurement system which will cause the measurement slightly lower than reality. Therefore, selection of the current barrier setup is a compromise between the eccentric loading and inertial effect of the measurement system. Two laser sensors were installed to measure the translation of the aluminum plate. Laser sensor 1 measures displacement at the top right corner of the aluminum plate while laser sensor 2 measures the displacement of the bottom left corner (Fig. 2). The data logger sampled data at 2000 Hz. Based on the known stiffness of the barrier system, the total impact force can be deduced for further analysis.

Test program and granular materials

To study the effects of water content on the dynamic impact behavior, different granular flows were modeled within the flume at a channel inclination of 35°. Three granular materials, completely decomposed granite (CDG, a non-uniform sandy soil), LB sand fraction C, and LB sand fraction E were adopted. Table 1 provides a summary of the test program.

Figure 3 shows the particle size distributions of each granular material. The water content was varied within the unsaturated range as 0, 10, 20, and 30%. Based on a reference void ratio, the corresponding degree of saturation and estimated matric suction of each material are summarized in Table 1. The total soil mass was kept constant (30 kg).

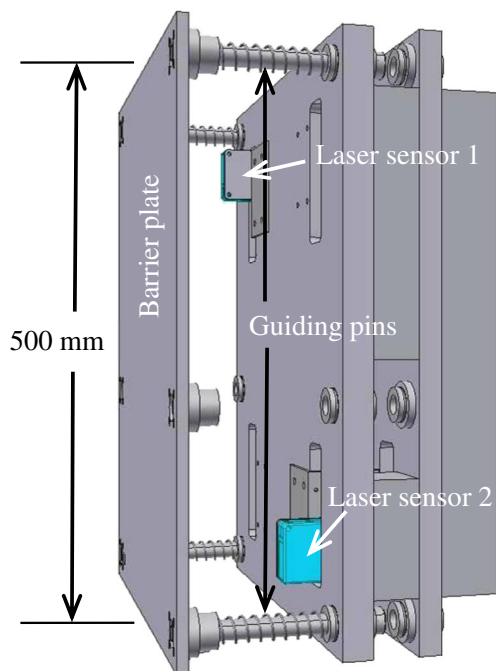


Fig. 2 Configuration of the barrier system

Testing procedures

The granular material was fully mixed with water and poured into the hopper just before tests to minimize consolidation and segregation. For granular soils in the unsaturated range, the solid particles form the skeleton of the mixture and water only partially fills the voids. The formation of “liquid bridge” between solid particles makes a much more twisty flow path of water than the saturated situation. As a result, the unsaturated mixture has a much lower permeability (difference about one order). Therefore, the time of soil-water separation of unsaturated mixtures should be much longer than that the saturated cases and the mixtures within the hopper were assumed to be homogenous before release.

After the gate was released to initiate a dam break failure, the mixture flowed downslope and impacted the barrier. Deformation of the barrier with respect to the impact time was recorded by laser sensors. Kinematics of the granular impact was captured by the high-speed camera.

Impact process of non-uniform completely decomposed granite (cdg) soil

Reverse segregation of dry CDG flows

Figure 4 shows the impact process of dry CDG particles (test CDGo, Table 1) upon impact with the barrier. The flow direction is from left to right. The impact time, T_i is reset to zero once the flow contacts the barrier. Impact kinematics (particle trajectories) is captured on the left and corresponding PIV analyses are shown on the right. The impact process can be characterized into two distinct stages. In the first stage, particle bouncing and collision dominate. Due to the longitudinal segregation of granular flows (Johnson et al. 2012), coarse particles that have accumulated at the flow front travel faster with frontal velocity 3.6 m/s (Table 1) and impact the barrier first. Afterwards, the coarser particles rebound and further become buried by subsequent fine particles. Figure 4a shows particles colliding frequently and randomly in front of the barrier. A cloud of fine particles due to the breakage of coarse particles can be observed (inset of Fig. 4a). Figure 4b shows subsequent flow accumulating at the base of barrier. The accumulation, a dead zone, forms and enlarges as more material reaches the barrier (Choi et al. 2015; Ng et al. 2016). Both the deposit height and length are developed in front of the barrier (Fig. 4b). Due to strong particle interactions, coarse particles are pushed upwards (PIV of Fig. 4b) while fine particles fall within the body of the granular assembly.

In the second stage, after the deposit reaching a certain height, subsequent descending particles slam into and flow over the previously deposited CDG (Fig. 4c). The flow velocity remains high on the free surface and attenuates quickly towards the inner side of the granular body (dead zone). The observed impact mechanism is reminiscent of pile-up mechanism as described by Choi et al. (2015). A pronounced shear zone develops at the free surface. This allows the fine particles to penetrate through the voids into the dead zone while leaving coarse particles at the free surface. The observed phenomenon is quite similar to “kinetic sieving” as illustrated by Savage and Lun (1988). Figure 4d shows that the length of deposited CDG is further elongated, where two angles (α and β for the elongated deposit) are defined for further interpretation.

Table 1 Test program for impact behavior of different granular materials

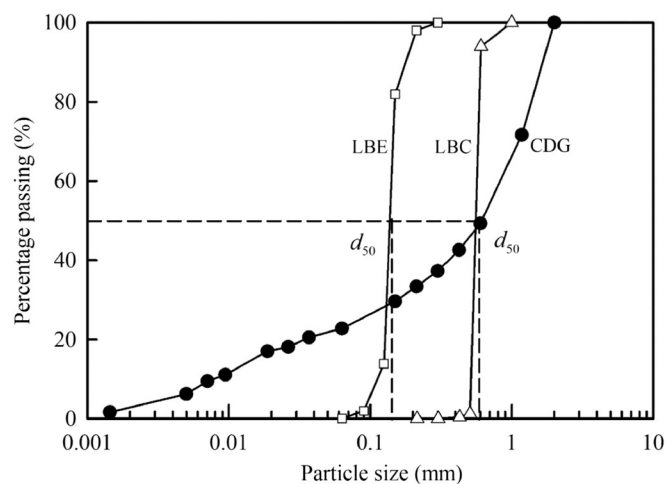
Test ID	Granular material	Water content (%)	Reference void ratio (solid fraction)	Estimated degree of saturation	Estimated suction (kPa)	Estimated frontal velocity (m/s)	Flow and impact pattern
CDG0	CDG (completely decomposed granite)	0	0.89 (0.47)	0.00	–	3.6	Progressive
CDG10		10		0.30	85.0	1.7	Transitional
CDG20		20		0.60	19.1	0.8	Discrete-surge
CDG30		30		0.90	4.8	0.5	Discrete-surge
LBC0	LB sand fraction C	0	0.82 (0.45)	0.00	–	4.2	Progressive
LBC10		10		0.32	1.6	2.7	Transitional
LBC20		20		0.65	0.7	3.6	Discrete-surge
LBC30		30		0.97	0.2	4.0	Discrete-surge
LBE0	LB sand fraction E	0	0.82 (0.45)	0.00	–	3.8	Progressive
LBE10		10		0.32	9.9	3.1	–
LBE20		20		0.65	4.0	2.4	Discrete-surge
LBE30		30		0.97	0.7	0.5	Discrete-surge

At the completion of impact process, a sectional view clearly demonstrates the reverse segregation of dry CDG (Fig. 5). The dashed line denotes the boundary whereby coarse particles accumulate at the free surface and fine grains move into the granular assembly. Bagnold (1954) use the term “dispersive stress” induced by shearing and Middleton (1970) adopted “kinetic sieving” to explain the mechanism of reverse segregation. Reverse segregation in the two stages presented suggests that both mechanical (shearing and collision) and geometric (kinetic sieving) effects are involved in the impact and deposition process. However, it is evident that a more comprehensive explanation of the mechanism is warranted (Zhou and Ng 2010).

Impact height and angle of dry CDG flows

Figure 4d shows CDG particles impacting the barrier and depositing at the base of the barrier, in a similar manner as that observed from the flume tests using dry quartz sand by Pudasaini et al.

(2007). Once the particles at the front of the flow impact the barrier, the rebound of particles become attenuated as a dead zone forms. The impact height H_{Impact} is largest at the barrier and decreases as it moves towards to shock that propagates towards the upstream direction. The shock is diffusive (Pudasaini et al. 2007), which means that the transition from the approaching supercritical flow with finite flow depth to a dead zone with larger thickness is not abrupt but smooth. The transition can be characterized with an S-shaped profile at the free surface (Fig. 4c). The direction of the motion changes dramatically as particles move from the thin flowing layer to form a granular jump. A granular jump is characterized as the rapid transition from slope-parallel motion to an essentially slope-perpendicular direction. Approaching particles climb the steep rear end of the dead zone at considerable speed and comes to rest soon after reaching the upper flank of the dead zone. The rear end the dead zone propagates upslope. Taking the intercept of the tangents connecting the

**Fig. 3** Particle size distributions of CDG soil and LB sands (fraction C and E)

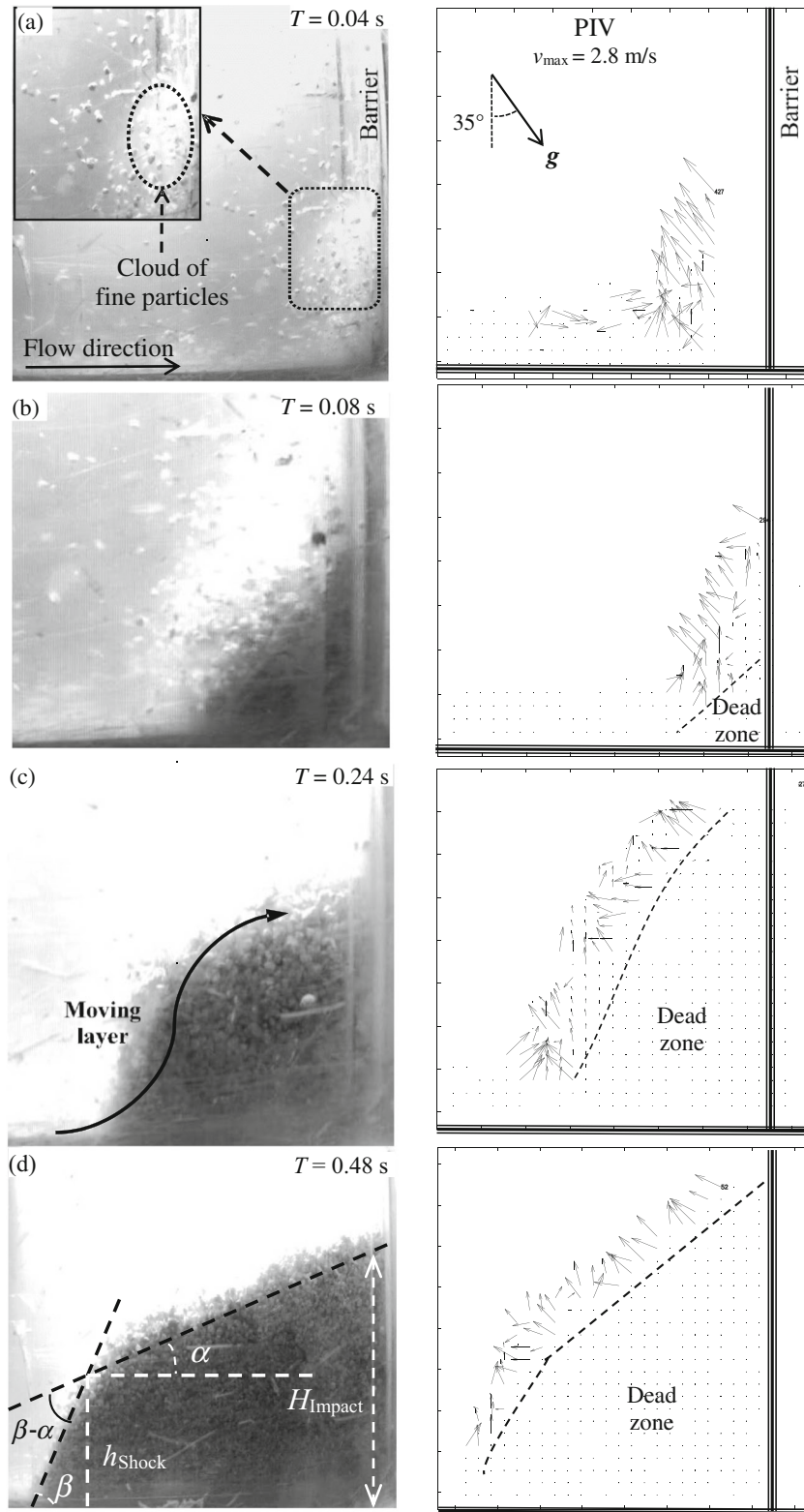


Fig. 4 Impact process of dry CDG (test CDG0)

frontal and rear slopes of the dead zone, the shock front height h_{Shock} is defined to be the distance from this point to the slope bed (Fig. 4d).

The kinematics of the dead zone and the shock are observed through the side wall. The angles α and β are defined between the two free surfaces of deposited CDG and the channel bed (Fig. 4d).

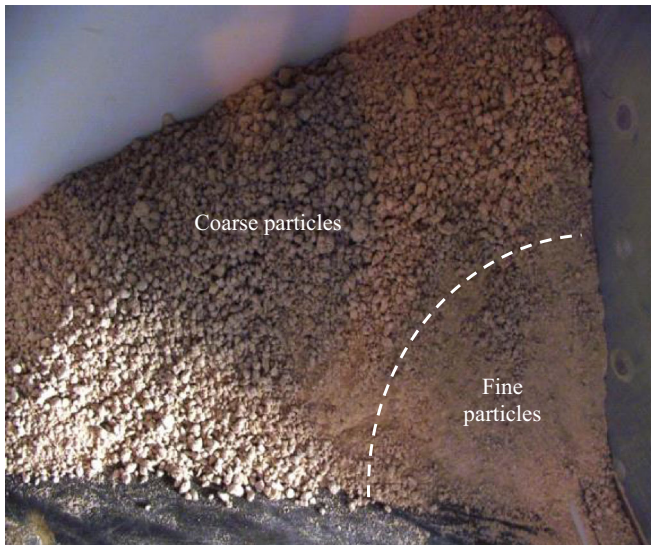


Fig. 5 Final deposition of dry CDG (test CDG0)

The impact process is further quantified through the variation of angles α and β , impact height H_{Impact} , and the height of the shock h_{Shock} (Fig. 6a, b). Initially during phase I, the angle α of the dead zone decreases significantly as the deposition increase along the flow direction. Angle β of the shock increases drastically compared to angle α (Fig. 6a). Particles within the shock collide with the previously deposited CDG and climbs upward along the steeper shock. The transition angle ($\beta-\alpha$) between two free surfaces also increases as the impact process progresses.

With the continuous development of a granular dead zone in front of the barrier and the granular shock propagating upslope, the impact height H_{Impact} and the shock height h_{Shock} increase gradually (Fig. 6b). After angle β of the shock reaches its peak value, both α and β decrease in phase II of the impact process and keep fluctuating almost synchronously (Fig. 6a). The transition of the impact shock to the deposited granular body (with S-shaped) becomes smoother as the measured transition angle ($\beta-\alpha$) decreases. Accordingly, Fig. 6b shows that during phase II of the impact process, the impact height H_{Impact} and shock height h_{Shock} further increase. In the last phase (III) of the impact process, the impact height H_{Impact} on barrier approaches a constant value while the shock height h_{Shock} drops before reaching an ultimate value. Angles α and β fluctuate in phase III, but the transition angle ($\beta-\alpha$) remains unchanged.

Impact behavior of wet CDG flows

Wet CDG soils with varying water contents (Table 1) were adopted to investigate the effects of water content on impact behavior. Figure 7 shows the flow pattern of CDG with a water content of 20%. Rather than the progressive accumulation observed using dry CDG, discrete surges are observed. Small clusters of wet particles impact the barrier and deposit (Fig. 8a, b), afterwards, a considerable proportion of the granular materials impacts the barrier (first and second surges in Fig. 7; see PIV result in Fig. 8c, d). These discrete surges are also responsible for inducing more pronounced barrier response. The subsequent massive flow climbs upwards along the free surface of the previously deposited CDG, resulting

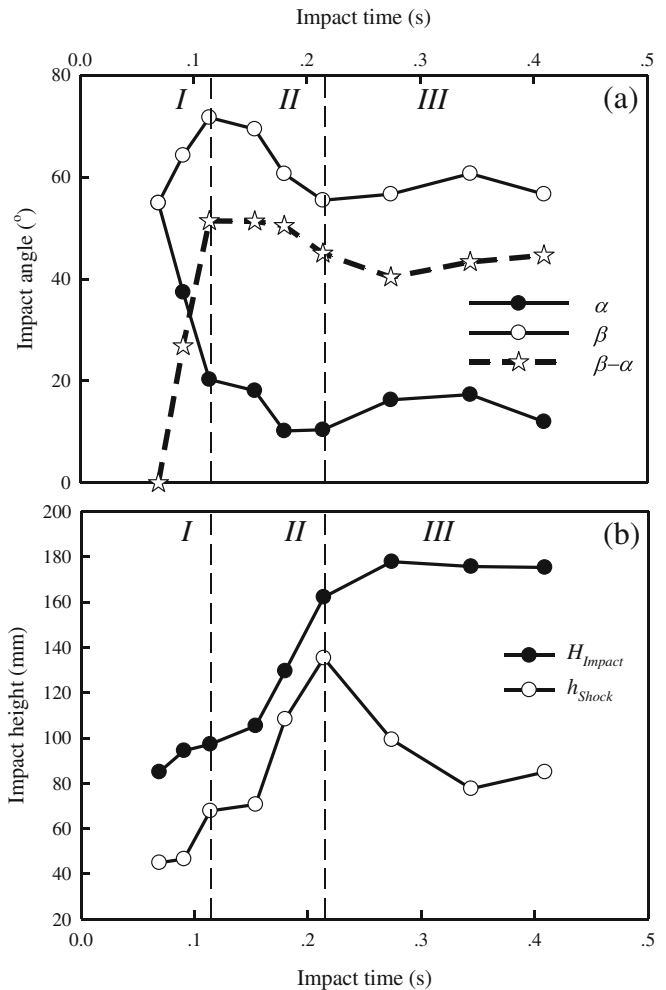


Fig. 6 Variation of a impact angle and b impact height with respect to impact time in front of the barrier

in much higher impact height. Compared with the kinematics observed for dry CDG flows, collisional behavior of wet CDG particles is not obvious.

Response of the barrier under impact of different water contents is shown in Fig. 9. The impact force of dry CDG particles on the barrier progressively increases and reflects the progressive accumulation of dry CDG. Owing to the effects of interstitial fluid among the wet solid particles, the induced matric suction

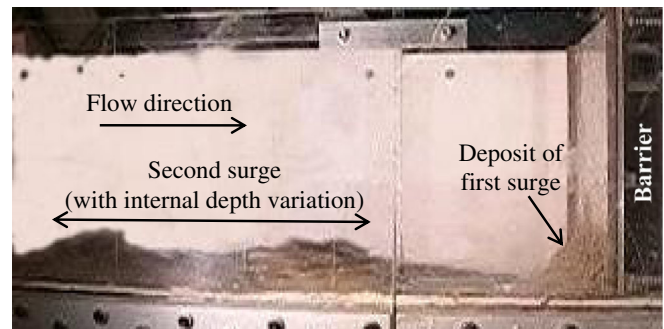


Fig. 7 Surge flow pattern of CDG with 20% water content (test CDG20)

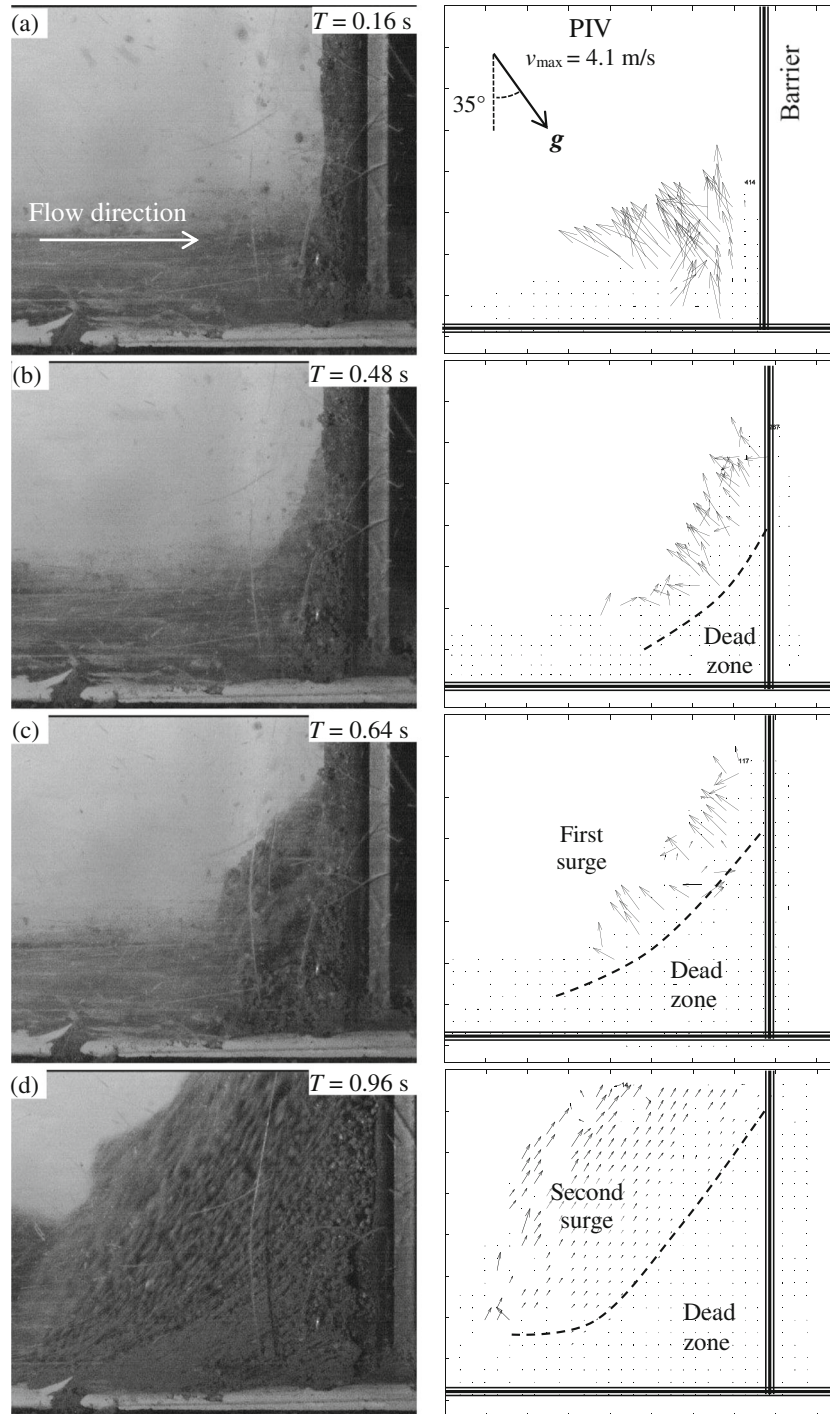


Fig. 8 Impact process of CDG with 20% water content (test CDG20)

enhances the shear strength (Fredlund et al. 1978) within the granular body and at the interface. The enhanced matric suction undoubtedly influences the mobility of the flow (Zhou et al. 2016). On the other hand, matric suction within the granular mass acts as an apparent cohesion and causes the fine particles to agglomerate together as clusters of particles. To overcome the enhanced shear strength caused by matric suction and to increase the downslope driving force, the wet granular mass self-organizes into “batches”

to increase the local flow depth (high depth gradient $\partial h/\partial s$). The depth gradient results in an unbalanced pressure force ΔP equal to the difference between the areas of the two triangles ($P_1 - P_2$) in Fig. 10. ΔP further equals $k\rho gh(\partial h/\partial s)\cos\theta$ (Hungry 1995), where k is lateral earth pressure coefficient in soil mechanics. The higher the depth gradient $\partial h/\partial s$ (local flow depth), the stronger the down-driving force on the surge flows. As a result of matric suction, wet CDG flows downward and interacts with the barrier in the form of

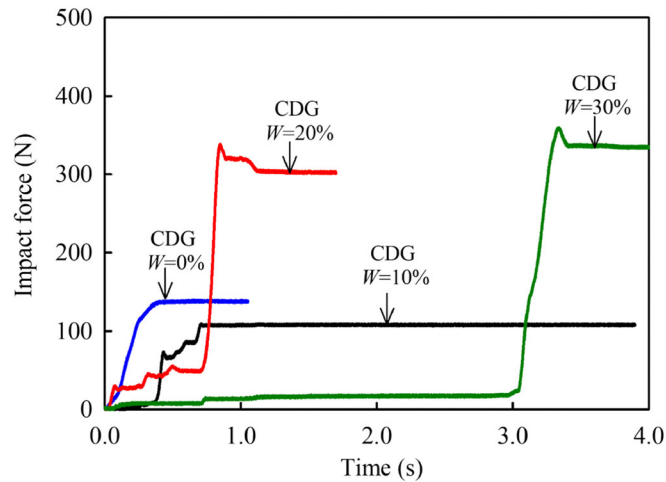


Fig. 9 Response of barrier to the impact of CDG with different water contents

discrete surges. For flows with discrete surges (e.g., water content of 20 or 30%), the impact force drop (difference between peak and static forces) and the duration of impact process (interval between surges) both increase (Fig. 9).

Impact process of uniform sands

LB sand fraction C

Figure 11 shows the impact process of dry LB sand fraction C (test LBCo) and the corresponding PIV analysis results. In general, the granular particles compact closely and the impact process occurs in a continuous manner. The dashed lines in the left column depict the free surface of the granular body at time interval $\Delta T = 0.16$ s. The dashed lines in the right column depict the boundary between the moving layer and the dead zone. When the first surge reaches the barrier at $T = 0.08$ s, the sand starts to accumulate at the base of the barrier. Both the impact height and dead zone length along the flow direction gradually develop (pile-up mechanism, Choi et al. 2015). At time of $T = 0.40$ s, the subsequent particles are

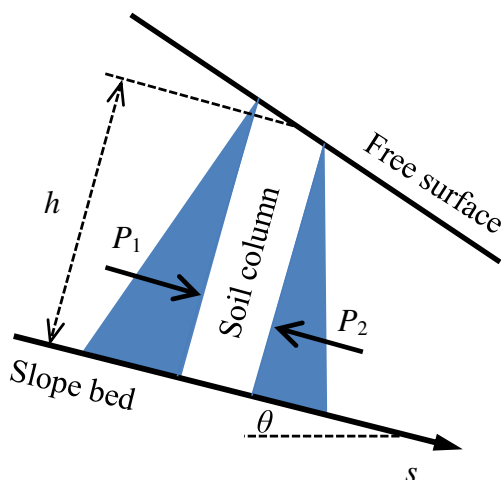


Fig. 10 Lateral earth pressure difference $\Delta P (=P_1-P_2)$ induced by depth gradient $\partial h/\partial s$ based on the depth integration theory (after Hungr 1995)

observed to impact against the rear end of dead zone. The avalanche length along the travel direction is further enhanced while the impact height remains unchanged because the subsequent flow cannot directly impact the barrier. The barrier is continuously loaded until a static state is reached. The free surfaces of the granular body are compared together in Fig. 11d and it is apparent that the distances between the dashed lines are fairly consistent. This implies a progressive accumulation of the granular material and an elongated impact time. As a result, the impact force is dominated by static loading (Ng et al. 2016) since the rate of momentum change is low for the progressive accumulation of sand against the barrier (pile-up mechanism).

Figure 12 shows the impact behavior of LB sand fraction C with a water content of 30% (test LBC30). By contrast to the progressive accumulation of dry granular flow (test LBCo), the sand mixed with water impacts on the barrier in discrete surges. The dynamic response of the barrier to solid-water mixtures is shown in Fig. 13. The greatest mass and momentum of the mixture concentrate in the second surge with a shortened impact duration (see high-speed photography and PIV analyses in Fig. 12c, d). Therefore, the impact force exhibits an impulse and the large deformation of the barrier saturates the laser sensors. By contrast, the barrier deforms progressively in the tests of lower water contents (e.g., 0 and 10%).

LB sand fraction E

Figure 14 depicts the impact behavior of LB sand fraction E. The impact process of the dry LB sand fraction E (test LBEo) is similar to that of dry LB sand fraction C (test LBCo). Generally, for the progressive accumulation (pile-up mechanism) of dry LB sand fraction E, the measured impact force gradually increases in multiple stages until $T = 1.1$ s, without exhibiting sharp impulses. Afterwards, the measured force reaches a static state. The duration is longer for fraction E compared to fraction C. Impact force drop is also observed for the mixtures of LB sand fraction E and water. However, the measured impact force induced by LB sand fraction E is much smaller in magnitude. A larger amount of wet sand perches on the slope channel due to the high matric suction induced by the relative fine sand. These mixtures actually do not impact on the barrier directly. As a result, the whole flow and

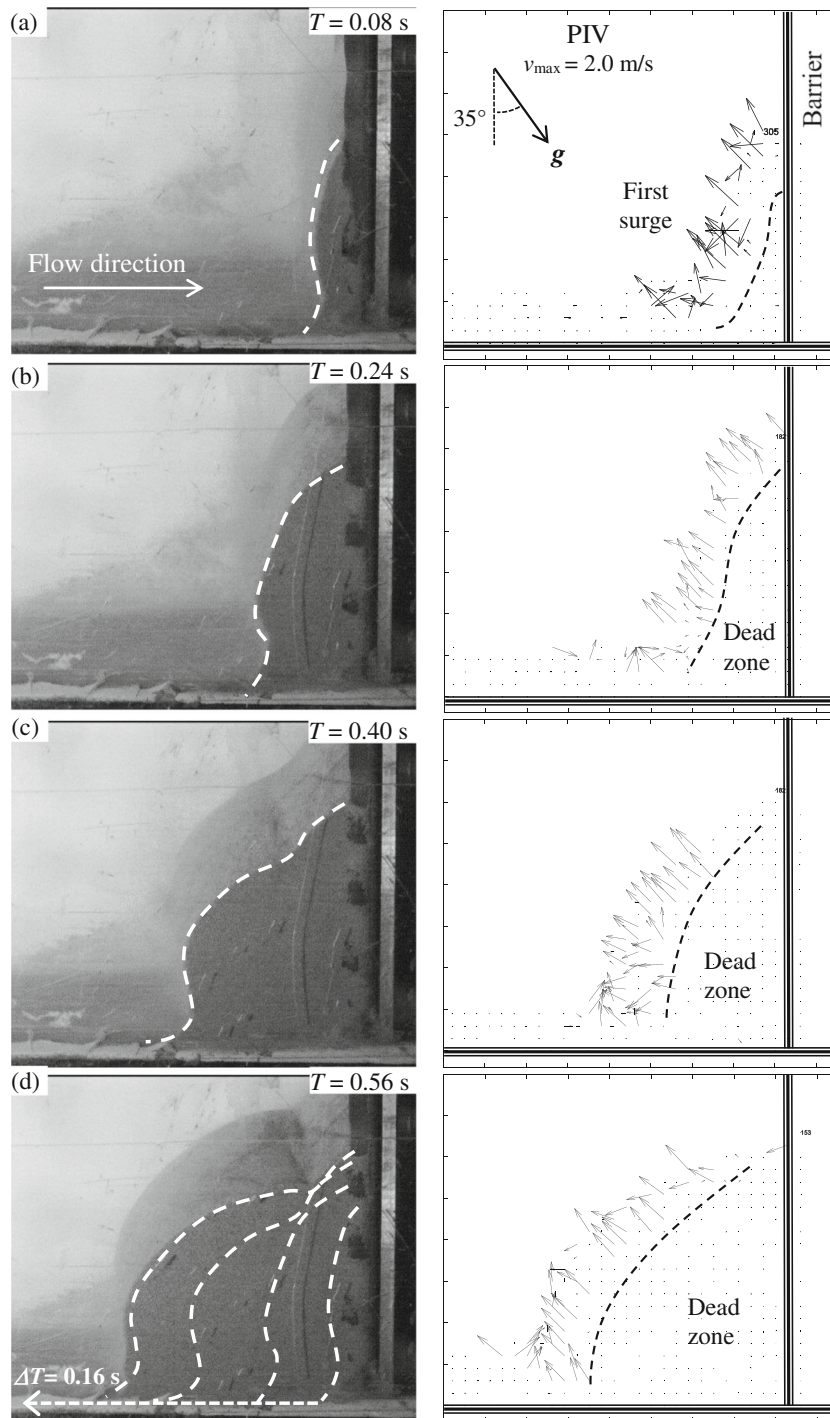


Fig. 11 Impact process of dry LB sand fraction C (test LBC0)

impact processes are not continuous. The effects of suction within fine materials are further discussed in the next section.

Effects of water content

Peak impact induced by discrete surges

The dry granular flows of CDG and uniform sands (LB sands fraction C and E) result in a progressive impact, characterized as

a “hardening” pattern of the impact force time histories. While the flows with higher water contents result in time histories with impulses induced by discrete surges (Figs. 9, 13, and 14). To further investigate the effects of water content on the impact behavior, the ratio of the maximum impact force and static loading of CDG and LB sands fraction C and E are plotted against the water content in Fig. 15a. Except the impact of LB sand fraction C with 30% water content (LBC₃₀) which reaches the upper limit of the

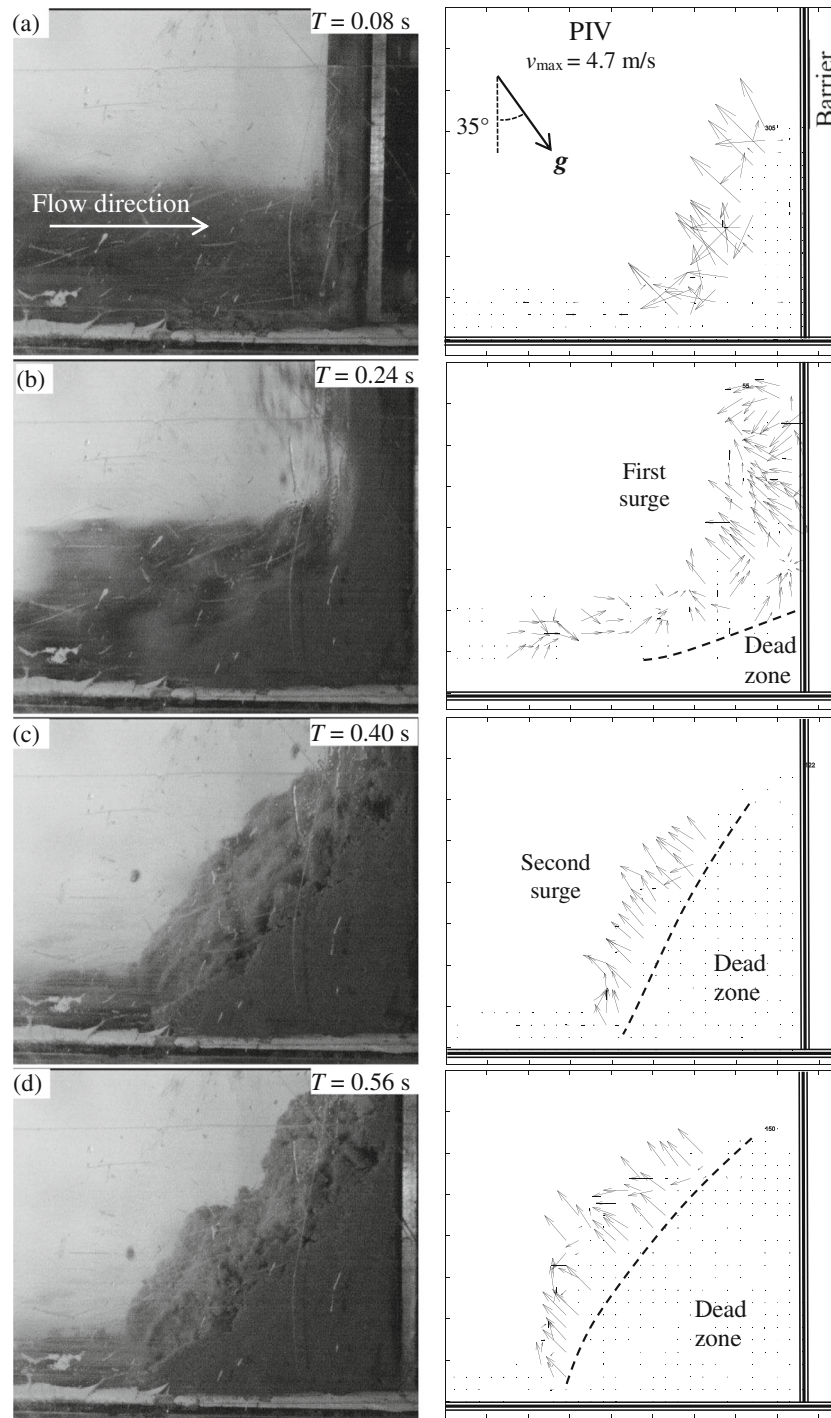


Fig. 12 Impact process of LB sand fraction C with 30% water content (test LBC30)

measurement, the peak-static ratio generally increases with the water content. This implies that the majority of momentum change of the flows with high water contents (20 and 30%) are concentrated within surges that interact with the barrier with short durations. The higher the peak-static ratio, the more dynamic the impact behavior. On the contrary, the granular flows with low water contents (0 and 10%) are characterized as continuous flows with finite depth and elongated impact duration. Although the dry

granular flows are characterized with relatively high frontal velocity (Table 1), the dynamic effect is not obvious and the static loading induced by the dead zone dominates the total impact force.

It has been widely accepted that the matric suction inside the granular flow body would enhance the mobilized shear strength (Fredlund et al. 1978) and thus the mobility would decrease accordingly. The flow mobility using the same soil, LB sand

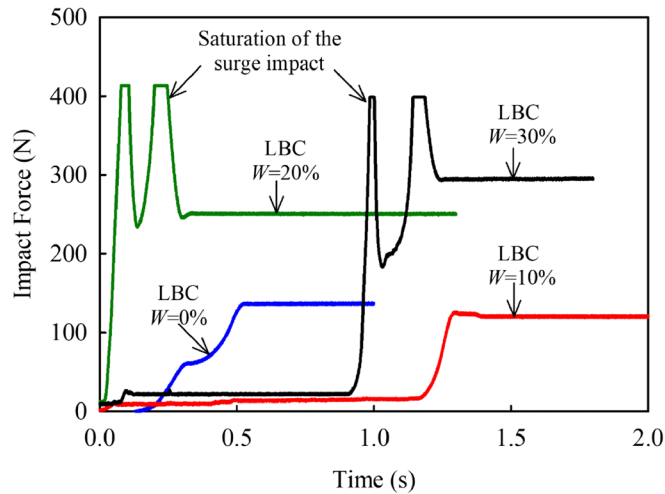


Fig. 13 Response of barrier to the impact of LB sand fraction C with different water contents

fraction C (Zhou et al. 2016), is adopted here to further illustrate the effect of discrete surges on the extraordinary loading behavior (Fig. 15b). From the unsaturated soil mechanics, as the water content is extremely low, the “liquid bridge” cannot form, thus the granular material behaves like air-saturated flow. On the other hand, as the water content approaches saturation, the matric suction plays negligible role in the dynamic properties, thus the flow behavior is close to that of water-saturated flows. There is an optimized water content (20% in Fig. 15b) where the matric suction exerts its maximum, denoting the highest shear strength and lowest mobility (highest travel angle, see the inset figure of Fig. 15b for physical meaning). Findings of this study, however, are out of expectation, because the dynamic loading effect is even obvious with the high suction effect considered. To overcome the additional shear strength from matric suction, the unsaturated granular flows form discrete surges (Zanuttigh and Lamberti 2007; Iverson et al. 2010) with high momentum transfer rate. This self-organization phenomenon (Bak 1996) should attract the attention of the geologists and the engineers who design retaining structures for the geophysical flow disasters.

Suction number and implication to the scale effect

As the dry granular flows transition towards saturated condition, an intermediate unsaturated flow state must exist. Unsaturated flows are characterized by enhanced internal shear strength due to the additional contact stress induced by the surface tension of water. Matric suction, acting as a type of apparent cohesion among the granules, is unlikely to be disturbed by large deformation since meniscus bridges can be reformed (Song et al. 2017). The existence of the suction effect further influences flow mobility (Zhou et al. 2016) and impact behavior by regulating the shear resistance of the flow.

Here, the dimensionless index suction number N_{suc} proposed by Song et al. (2017) is adopted to quantify the suction effect over frictional shearing:

$$N_{suc} = \frac{\psi}{\rho gh} \quad (1)$$

where ψ is the matric suction (Pa) and ρgh denotes the overburden pressure (Pa) induced by flow depth h (m). Physically, the

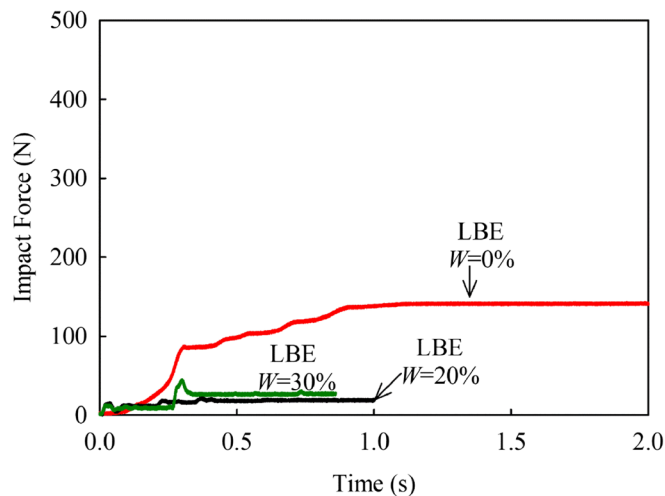


Fig. 14 Response of barrier to the impact of LB sand fraction E with different water contents

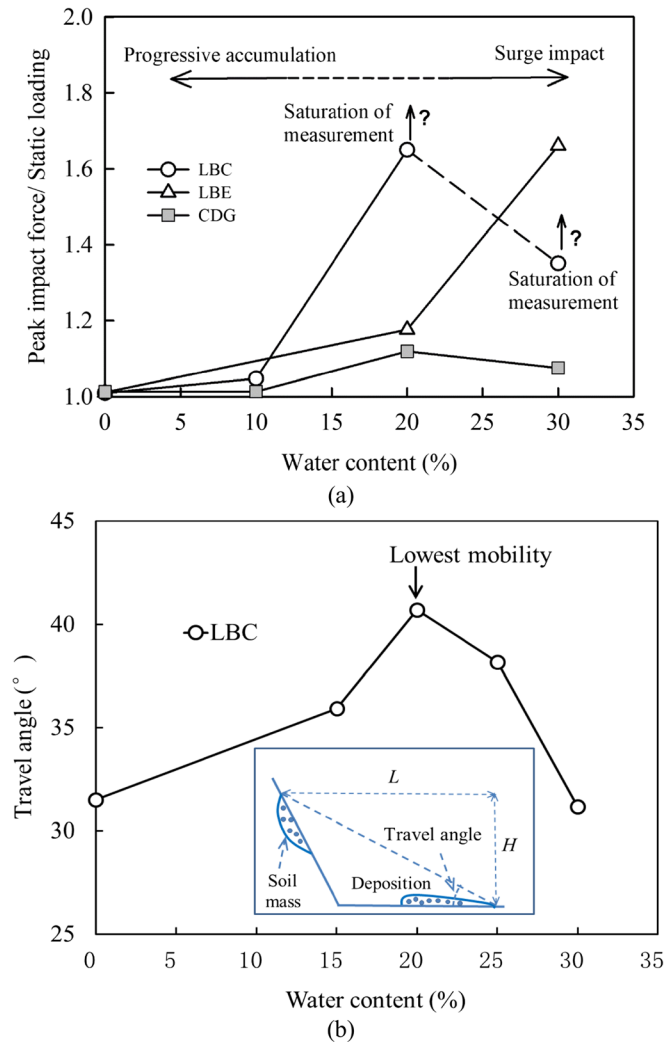


Fig. 15 Effect of water content on a peak impact forces for different granular materials; **b** flow mobility of LB sand fraction C (after Zhou et al. 2016), definition of travel angle is shown in the inset figure

maximum matric suction ψ_{\max} (Pa) corresponds to the minimum pore radius r_{\min} (m):

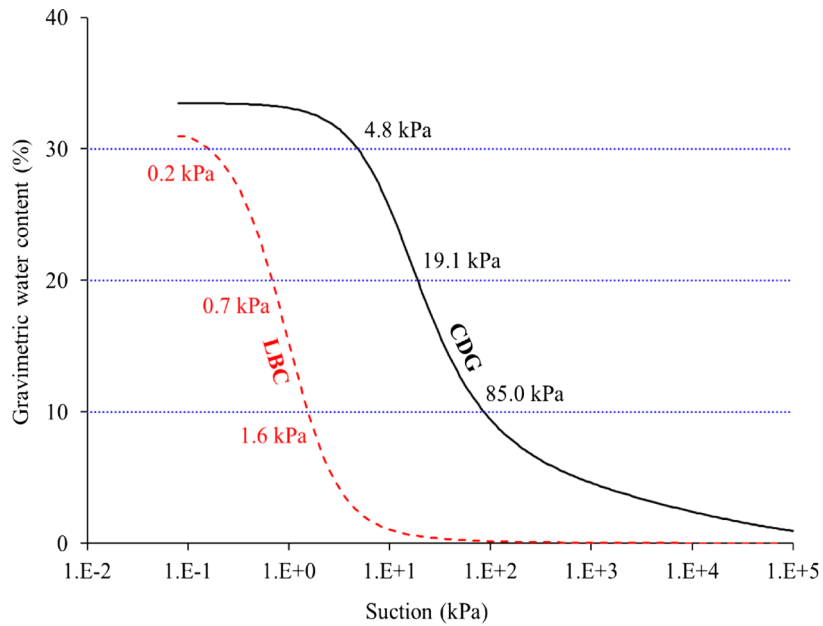
$$\psi_{\max} = \frac{2T_s \cos \alpha_{ws}}{r_{\min}} \quad (2)$$

where T_s is the surface tension of water (N/m) and α_{ws} is contact angle between water and soil.

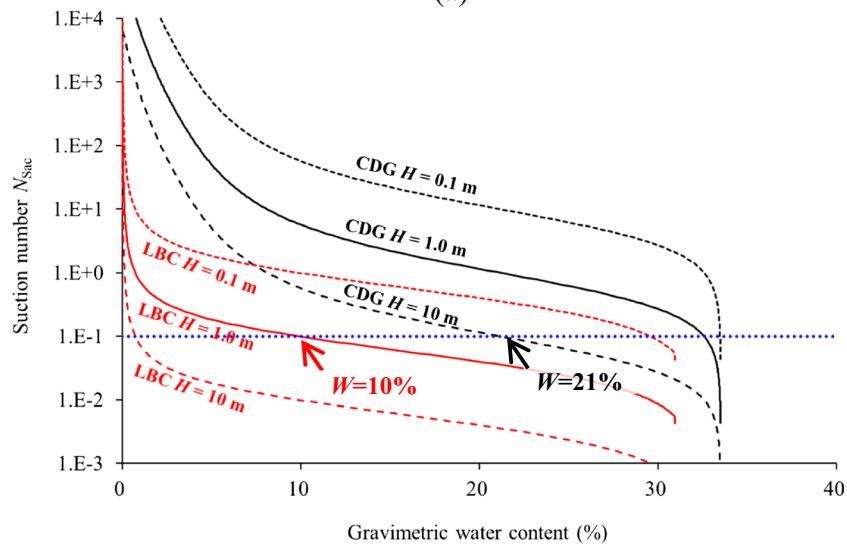
According to Eq. (2), once fine particles, like clays and silts which can fill up the large voids formed by coarse particles, are introduced into the flows, the effect of suction starts to play an impact role. The CDG soil and LB sand fraction C have a close mean grain size d_{50} (Fig. 3). However, owing to the large amount of clay and silt in the non-uniform CDG soil, the induced suction (soil-water characteristic curve, Fig. 16a) and the dynamics (suction number, Fig. 16b) are quite different from those of LB sand fraction C. Figure 16a shows the soil-water characteristic curve (SWCC) for CDG and LB sand fraction C. The SWCC curves are estimated based on the model

proposed by Fredlund et al. (2002). For a specific soil, the soil-water characteristic curve (SWCC) can be predicted using the particle size distribution and void ratio. Note the suction number is the ratio between the matric suction ψ and the overburden stress ρgh . Accordingly, the relationship between suction number N_{suc} and water content for CDG and LB sand fraction C at specific flow depth h can be deduced (Fig. 16b). The effect of suction for CDG is much higher than that on the uniform coarse LB sands. Furthermore, the S-shaped curves for CDG soil are much steeper, denoting the higher sensitivity of suction to the water content. For LB sand fraction C, however, the influence of water content to the overall suction is relatively constant.

The scale effect, i.e., effect of suction on the dynamic behavior of granular flows at different flow depths, can also be inferred by comparing the suction number at flow depths of 0.1, 1.0, and 10 m (Fig. 16b). For uniform coarse sand with depth of 1.0 m, the induced suction is less dominant on the flow dynamics ($N_{\text{suc}} < 0.1$) for most part of the unsaturated water content range (water content higher than 10%). For soils



(a)



(b)

Fig. 16 a SWCC (soil-water characteristics curve) of CDG and LB sand fraction C, for SWCC curve, the suction value locates in the ordinate. b Relationship between the suction number and water content

with substantial fine particles, like the CDG, even with flow depth of 10 m, the effect of suction cannot be neglected at water content less than 21% (Fig. 16b). This study is carried out with flow depth of about 0.1 m; therefore, the dynamics (mobility and impact behavior) is unexpectedly affected by the matrix suction.

In this study, the reference void ratios (Table 1) based on the prepared samples are adopted to estimate the suction at varying water content (SWCC). However, under high-speed movement, the shear-induced volumetric change (dilation) would result in change in pore size and pore distribution. Therefore, suction would change accordingly. Currently, there have already existed granular flow models to quantify the volumetric change on dry

and fully saturated flows (Andreotti et al. 2013; Iverson and George 2014). For quasi-static soil mechanics, the evaluation of volumetric change of unsaturated soils has been developed based on the framework of critical state soil mechanics (Chiu and Ng 2003). Yet, the physically based models, considering the shear-induced dilation and self-organization of discrete surges in the unsaturated range, have not been developed. As a preliminary investigation of the suction effect, the results of this study are still of guiding significance to the understanding of unsaturated geophysical flow impact behavior. Furthermore, the proposed suction number could be a useful index for design and scaling of model tests and for cost-effective design of protection engineering.

Conclusions

Flume experiments investigating the effects of water content of granular flows on the dynamic response of an instrumented barrier were carried out. The impact behavior between uniform and non-uniform solid particles was compared. More specifically, the unsaturated properties of geophysical flows with varying depths were investigated in a dimensionless approach. Key conclusions are drawn as follows:

1. The impact process of dry non-uniform CDG flows on the barrier can be characterized into two distinct stages. In the first stage, coarse particles break upon collision with the barrier. The coarse particles then flow upwards and accumulate near the free surface of the deposited granular body while fine particles are squeezed into the dead zone. In the second stage, strong shearing develops within the layer near the free surface of the enlarging dead zone. During this process, fine particles penetrate through the voids formed by coarse particles. Both mechanical (shearing and collision) and geometric (kinetic sieving) effects account for the reverse segregation in an impact scenario for dry granular flows with non-uniform particle size.
2. The impact kinematics and dynamics of granular flows are strongly influenced by the water content. When the water content is low (e.g., 0 and 10%), the sharp impulses are not manifested in the dynamic response of the barrier, which corresponds to the progressive accumulation of granular material. This indicates that the loading process is dominated by the static load induced by dead zone. On the contrary, for higher water contents (e.g., 20% and 30%), discrete surges, rather than progressive accumulation, are observed to impact on the barrier. The surge impact results in sharp impulses in the impact force time history.
3. The matric suction enhances the mobilized shear strength and thus reduces the mobility of unsaturated granular flows. However, from the findings of this study, the dynamic loading effect (impulses) is even obvious with matric suction considered. To overcome the enhanced shear strength from matric suction and to increase the downslope driving force, self-organization of the wet granular mass is observed. Self-organization increases the local flow depth (high depth gradient) and thus the lateral spreading pressure. Therefore, unsaturated soils flow downward and interact with the barrier in the form of discrete surges with enhanced momentum transfer.
4. A new dimensionless parameter, suction number, is used to quantify the effect of suction on the dynamic behavior of granular flows with different flow depths. For soils with substantial fine content, the effect of suction still cannot be neglected for large-scale geophysical flows (up to 10 m depth). The suction number serves as a useful index for design and scaling of model tests and understanding of the dynamics of natural geophysical flows.

Acknowledgements

The authors would like to thank the HKUST Jockey Club Institute for Advanced Study for their support.

Funding information The authors acknowledge the support from the National Natural Science Foundation of China (grant no.

11672318), the Key Research Program of Frontier Sciences, Chinese Academy of Sciences (CAS) (grant no. QYZDB-SSW-DQC010), the research grant T22-603/15-N provided by the Research Grants Council of the Government of Hong Kong SAR, China, and the International Partnership Program of Chinese Academy of Sciences (grant no. 131551KY5B20160002). Moreover, the financial support from Youth Innovation Promotion Association CAS and CAS Pioneer Hundred Talents Program are also greatly appreciated.

References

- Andreotti B, Forterre Y, Pouliquen O (2013) *Granular media: between fluid and solid*. Cambridge University Press, Cambridge
- Armanini A, Capart H, Fraccarollo L, Larcher M (2005) Rheological stratification in experimental free-surface flows of granular-liquid mixtures. *J Fluid Mech* 532:269–319
- Armanini A, Fraccarollo L, Larcher M (2008) Liquid-granular channel flow dynamics. *Powder Technol* 182(2):218–227
- Bagnold RA (1954) Experiments on a gravity-free dispersion of large solid spheres in a Newtonian fluid under shear. *Proc R Soc Lond A: Math Phys Eng Sci* 225(1160):49–63
- Bak P (1996) *Complexity and criticality. In How nature works*. Springer, New York
- Bugnion L, McArdell BW, Bartelt P, Wendeler C (2012) Measurements of hillslope debris flow impact pressure on obstacles. *Landslides* 9(2):179–187
- Campbell CS (1990) Rapid granular flows. *Annu Rev Fluid Mech* 22(1):57–92
- Chen HX, Zhang LM, Zhang S, Xiang B, Wang XF (2013) Hybrid simulation of the initiation and runout characteristics of a catastrophic debris flow. *J Mt Sci* 10(2):219
- Chiu CF, Ng CWW (2003) A state-dependent elasto-plastic model for saturated and unsaturated soils. *Géotechnique* 53(9):809–830
- Choi CE, Au-Yeung SCH, Ng CWW, Song D (2015) Flume investigation of landslide granular debris and water runup mechanisms. *Géotechnique Lett* 5:28–32
- Da Cruz F, Emam S, Prochnow M, Roux JN, Chevoir F (2005) Rheophysics of dense granular materials: discrete simulation of plane shear flows. *Phys Rev E* 72(2):021309
- Davies TR, McSaveney MJ (1999) Runout of dry granular avalanches. *Can Geotech J* 36(2):313–320
- Fredlund DG, Morgenstern NR, Widger RA (1978) The shear strength of unsaturated soils. *Can Geotech J* 15(3):313–321
- Fredlund MD, Wilson GW, Fredlund DG (2002) Use of the grain-size distribution for estimation of the soil-water characteristic curve. *Can Geotech J* 39(5):1103–1117
- Goldhirsch I (2003) Rapid granular flows. *Annu Rev Fluid Mech* 35:267–293
- Gray JMNT, Chugunov VA (2006) Particle-size segregation and diffusive remixing in shallow granular avalanches. *J Fluid Mech* 569:365–398
- Hungr O (1995) A model for the runout analysis of rapid flow slides, debris flows, and avalanches. *Can Geotech J* 32(4):610–623
- Hungr O, Leroueil S, Picarelli L. The Varnes classification of landslide types, an update. *Landslides* (2014) 11: 167. <https://doi.org/10.1007/s10346-013-0436-y>
- Iverson RM (1997) The physics of debris flows. *Rev Geophys* 35(3):245–296
- Iverson RM, George DL (2014) A depth-averaged debris-flow model that includes the effects of evolving dilatancy. I. Physical basis. *Proc R Soc Lond A: Math Phys Eng Sci* 470(2170):20130819
- Iverson RM, Vallance JW (2001) New views of granular mass flows. *Geology* 29(2):115–118
- Iverson RM, Logan M, LaHusen RG, Berti M (2010) The perfect debris flow? Aggregated results from 28 large-scale experiments. *J Geophys Res: Earth Surf* 115(F03005):29. <https://doi.org/10.1029/2009JF001514>
- Johnson CG, Kokelaar BP, Iverson RM, Logan M, LaHusen RG, Gray JMNT (2012) Grain-size segregation and levee formation in geophysical mass flows. *J Geophys Res* 117:F002185
- Koo RCH, Kwan JS, Ng CWW, Lam C, Choi CE, Song D, Pun WK (2017) Velocity attenuation of debris flows and a new momentum-based load model for rigid barriers. *Landslides* 14(2):617–629
- Kwan JSH, Chan SL, Cheuk JCY, Koo RCH (2014) A case study on an open hillside landslide impacting on a flexible rockfall barrier at Jordan Valley, Hong Kong. *Landslides* 11(6):1037–1050
- Law RPH, Choi CE, Ng CWW (2015) Discrete-element investigation of influence of granular debris flow baffles on rigid barrier impact. *Can Geotech J* 53(1):179–185
- Middleton G (1970) Experimental studies related to the problem of flysch sedimentation. *Geol Assoc Can Spec Pap* 7:253–272
- MiDi G (2004) On dense granular flows. *Eur Phys J E* 14(4):341–365
- Mills P, Loggia D, Tixier M (1999) Model for a stationary dense granular flow along an inclined wall. *EPL (Europhys Lett)* 45(6):733

- Ng CWW, Choi CE, Song D, Kwan JHS, Koo RCH, Shiu HYK, Ho KK (2015) Physical modeling of baffles influence on landslide debris mobility. *Landslides* 12(1):1–18
- Ng CWW, Song D, Choi CE, Liu LHD, Kwan JSH, Koo RCH, Pun WK (2016) Impact mechanisms of granular and viscous flows on rigid and flexible barriers. *Can Geotech J* 54(2):188–206
- Pudasaini SP, Hutter K, Hsiau SS, Tai SC, Wang Y, Katzenbach R (2007) Rapid flow of dry granular materials down inclined chutes impinging on rigid walls. *Phys Fluids* 19(5):053302
- Savage SB, Hutter K (1989) The motion of a finite mass of granular material down a rough incline. *J Fluid Mech* 199:177–215
- Savage SB, Lun CKK (1988) Particle size segregation in inclined chute flow of dry cohesionless granular solids. *J Fluid Mech* 189:311–335
- Savage SB, Sayed M (1984) Stresses developed by dry cohesionless granular materials sheared in an annular shear cell. *J Fluid Mech* 142:391–430
- Song D, Ng CWW, Choi CE, Zhou GGD, Kwan JSH, Koo RCH (2017) Influence of debris flow solid fraction on rigid barrier impact. *Can Geotech J*. <https://doi.org/10.1139/cgj-2016-0502>
- Take WA (2015) Thirty-sixth Canadian geotechnical colloquium: advances in visualization of geotechnical processes through digital image correlation. *Can Geotech J* 52(9):1199–1220
- Wendeler C (2016) Debris flow protection systems for mountain torrents—basic principles for planning and calculation of flexible barriers. *WSL Bericht* 44. ISSN 2296-3456
- White DJ, Take WA, Bolton MD (2003) Soil deformation measurement using particle image velocimetry (PIV) and photogrammetry. *Geotechnique* 53(7):619–631
- Zanuttigh B, Lamberti A (2007) Instability and surge development in debris flows. *Rev Geophys* 45:RG3006
- Zhou GGD, Ng CWW (2010) Numerical investigation of reverse segregation in debris flows by DEM. *Granul Matter* 12(5):507–516
- Zhou GGD, Wright NG, Sun Q, Cai Q (2016) Experimental study on the mobility of channelized granular mass flow. *Acta Geol Sin (Eng Ed)* 3:022

G. G. D. Zhou · D. Song (✉)

Key Laboratory of Mountain Hazards and Earth Surface Process/Institute of Mountain Hazards and Environment,
Chinese Academy of Sciences (CAS),
Chengdu, China

Email: drsong@imde.ac.cn

G. G. D. Zhou
e-mail: gordon@imde.ac.cn

G. G. D. Zhou · D. Song
University of Chinese Academy of Sciences,
Beijing, China

C. E. Choi
Department of Civil and Environmental Engineering,
The Hong Kong University of Science and Technology,
Clear Water Bay, Kowloon, Hong Kong
e-mail: ceclarence@ust.hk

C. E. Choi
The HKUST Jockey Club Institute for Advanced Study,
The Hong Kong University of Science and Technology,
Clear Water Bay, Kowloon, Hong Kong

A. Pasuto
Research Institute for Geological and Hydrological Hazard Prevention,
National Research Council of Italy,
Padova, Italy
e-mail: alessandro.pasuto@irpi.cnr.it

Q. C. Sun
State Key Laboratory for Hydrosience and Engineering,
Tsinghua University,
Beijing, China
e-mail: qcsun@tsinghua.edu.cn

D. F. Dai
Kunming Dongchuan Debris Flow Prevention and Control Institute,
Kunming, China
e-mail: 844532566@qq.com